Deformation behavior of an amorphous $Cu_{64.5}Zr_{35.5}$ alloy: A combined computer simulation and experimental study

M. I. Mendelev, R. T. Ott, M. Heggen, M. Feuerebacher, M. J. Kramer, and D. J. Sordelet

Citation: Journal of Applied Physics **104**, 123532 (2008);
View online: https://doi.org/10.1063/1.3043587
View Table of Contents: http://aip.scitation.org/toc/jap/104/12
Published by the American Institute of Physics

Deformation behavior of an amorphous $Cu_{64.5}Zr_{35.5}$ alloy: A combined computer simulation and experimental study

M. I. Mendelev,[1,a] R. T. Ott,[1] M. Heggen,[2] M. Feuerebacher,[2] M. J. Kramer,[1,3] and D. J. Sordelet[1]
[1]*Materials and Engineering Physics Program, Ames Laboratory, Ames, Iowa 50011, USA*
[2]*Institut fur Festkorperforschung, Forschungszentrum Jülich GmbH, 52428 Jülich, Germany*
[3]*Department of Materials Science and Engineering, Iowa State University, Ames, Iowa 50011, USA*

(Received 24 August 2008; accepted 31 October 2008; published online 30 December 2008)

Molecular dynamics (MD) simulations were performed to examine the temperature-dependent elastic properties and high-temperature deformation behavior of a $Cu_{64.5}Zr_{35.5}$ amorphous alloy. From the simulations we find that the elastic constants of the amorphous solid and supercooled liquid exhibit an approximately linear temperature dependence. The predicted temperature dependence of the Young's modulus for the amorphous solid obtained from the MD simulations is in good agreement with experimental measurements using dynamic mechanical analysis. Furthermore, the high-temperature plastic deformation behavior determined by MD simulations is qualitatively in good agreement with results from plastic deformation experiments performed on 1 mm diameter $Cu_{64.5}Zr_{35.5}$ metallic glass rods at 698 K. Notably, the MD simulations reveal that the flow softening regime of the stress-strain curve corresponds to an increase in the free volume in the atomic structure. Moreover, the simulations indicate that the atomic mobility significantly increases within the same regime. © *2008 American Institute of Physics*. [DOI: 10.1063/1.3043587]

I. INTRODUCTION

Numerous experimental studies have demonstrated the different deformation behaviors of metallic glasses.[1–7] At higher strain rates and lower temperatures, deformation becomes localized into shear bands, which under certain loading configurations can propagate uninterrupted through the material, causing catastrophic failure.[2,3] At lower strain rates and higher temperatures approaching the glass transition temperature of the specific alloy, the plastic strain is uniform in each volume element, and thus, the deformation is homogeneous.[6,8,9] While the elastoplastic response of metallic glasses can be measured very accurately, a clear physical understanding of the atomic displacements necessary to accommodate the deformation is still lacking.

In particular, irreversible plastic flow has been theorized to be associated with dilations within the disordered structure. This concept was presented phenomenologically by Spaepen[9] using the free volume theory of Cohen and Turnbull.[10] Spaepens's ideas have gained support through numerous studies, which collectively demonstrate that the mechanical behavior of metallic glasses is indeed strongly dependent on the atomic structure. For example, van den Beukel *et al.*[11] showed that structural relaxation, which they correlated with a reduction in free volume, significantly increased viscosity and stiffness. Alternatively, free volume has been shown to increase during high-temperature deformation,[12,13] allowing the system to recover ductility that is diminished following low temperature annealing. The atomistic mechanisms associated with free volume changes in metallic glasses are difficult to study experimentally. Molecular dynamics (MD) simulations, however, can be utilized to examine the evolving structure during deformation, particularly following yielding where plastic deformation can result in both an increase in free volume and localized structural transformations within the atomic structure. Falk and Langer[14] made a critical contribution toward understanding the deformation behavior of metallic glasses through their analysis of a two-dimensional, binary glass using Lennard-Jones potentials. Their numerical simulations were able to exhibit a transition from reversible elastic to irreversible plastic deformation; moreover, the stress state of their model system was found to be dependent on the history (e.g., degree of prior deformation) of the binary glass, implying that the atomic configuration at a specific time is directly linked to the deformation behavior. This point was recently addressed by Shi *et al.*[15] who correlated the deformation behavior, which in this case was limited to shear localization, with the atomic configuration. By quenching at different rates, they showed that their model binary glass was in contrasting degrees of structural relaxation, and furthermore, as more relaxation was allowed via slower quenching, the system exhibited greater propensity toward shear localization and shear band propagation.

Simulations using two-dimensional systems where atoms interact via the Lennard-Jones potential[14–16] have been very instructive for identifying dynamic and energetic contributions to metallic glass deformation. However, there is a very compelling need to perform simulations in three dimensions, and more importantly using interatomic potentials that describe the salient structural and thermodynamic properties of the alloy system. One approach is to utilize many-body, semiempirical, interatomic potentials such as the embedded atom method (EAM),[17] the EAM Finnis–Sinclair (FS) method,[18] or effective medium theory (EMT) (Ref. 19) to

[a]Author to whom correspondence should be addressed. Electronic mail: mendelev@ameslab.gov.

perform large-scale classical MD simulations. In addition, it is extremely desirable to simulate a system that can also be synthesized in the laboratory and tested experimentally to interrogate the predictions of the corresponding simulations. Correlating MD simulations with experimental measurements has garnered significant attention in the past few years, particularly following reports of enhanced glass formability in the Cu–Zr system.[20,21] Duan *et al.*[22] examined the atomic structure of a $Cu_{46}Zr_{54}$ metallic glass and compared bond distances and coordination numbers to experimental results obtained from quenched samples. Notably, they obtained rather large Cu–Cu bond distances in their simulated amorphous structure and attributed this to the substantially higher quench rate. This may be an appropriate conclusion, but nevertheless it clearly points to the need for optimizing the accuracy of interatomic potentials. This point was illustrated recently in another report discussing MD simulations of amorphous Cu–Zr. Paduraru *et al.*[23] utilized the EMT method to describe the structure of a $Cu_{50}Zr_{50}$ metallic glass. However, they did not report if their potential predicted fcc and hcp as the most stable lattices for pure Cu and Zr, respectively, at low temperature; furthermore, they did not indicate the ability of their potential to simulate the hcp-to-bcc transition for Zr.

A primary objective of MD simulations of noncrystalline materials using semiempirical interatomic potentials is to accurately describe structural properties that *were not used* in the fitting process for developing the potential. Additionally, it is clearly desirable for the potential to accurately reflect these properties over a wide range of compositions and temperatures, and further to mimic the mechanical response (e.g., elastoplastic deformation) of a real glass under different experimental conditions. If these criteria are met, simulations can provide valuable insights into complex phenomena that are either very difficult or essentially impossible to probe directly by experimental techniques. For instance, MD simulations of Cu–Zr glasses were performed to investigate the influences of temperature and configurational potential energy on elastic properties.[24] Similarly, MD simulations with simple pair potentials were utilized to examine the effects of alloy composition on the different degrees of free volume, as determined using Voronoi polyhedra analyses.[25]

We have recently developed a FS potential for the Cu–Zr system.[26] Potentials for pure Cu from Ref. 27 and pure Zr from Ref. 28 were included in the development of our Cu–Zr potential. Both elemental potentials accurately capture the salient crystalline properties and are in good agreement with experimental liquid diffraction data. Particularly important is that the Cu potential predicts that the fcc structure is the most stable phase for Cu from 0 K to the melting temperature. Furthermore, the Zr potential predicts that the hcp structure is the most stable phase in pure Zr at low temperature, and the bcc structure is the most stable phase at high temperature. The cross functions for the Cu–Zr potential were fit to first-principles data.[27] We recently demonstrated that MD simulations utilizing this potential can provide reasonable agreement with the experimentally measured compositional dependence of the room temperature Young's modulus for a series of amorphous Cu_xZr_{1-x} alloys.[29] It should be noted that *no* elastic constant data were utilized in the fitting procedure to develop this FS potential, so the agreement between simulation and experiment is encouraging. In the present study, this potential was used to examine the temperature dependence of the elastic constants for a $Cu_{64.5}Zr_{35.5}$ metallic glass. The comparison of the simulation results with experimental measurements of the Young's modulus further confirmed the reliability of this potential. The simulations were also utilized to calculate the Poisson's ratio and shear modulus as functions of temperature, which can be difficult to obtain experimentally for samples that can only be synthesized with cross-sectional dimensions of ~1 mm while maintaining a fully amorphous structure such as the $Cu_{64.5}Zr_{35.5}$ alloy used in the current study. Furthermore, we performed MD simulations of compressive deformation in a biaxial mode at 700 K. The mechanical response of the simulated glass is compared with experimental data obtained from a $Cu_{64.5}Zr_{35.5}$ metallic glass deformed at the same temperature. The analysis of the simulated structures during plastic deformation reveals that the evolution of free volume is dependent on both the plastic strain and the strain rate. Finally, we investigated the effect of plastic flow on the atomic mobility of Cu and Zr in the simulated metallic glass.

II. METHODS: COMPUTER SIMULATIONS AND EXPERIMENTAL TECHNIQUES

A. MD simulations

The FS potential developed in Ref. 26 was utilized for the MD simulations in the current study. As previously mentioned, we demonstrated that this potential accurately reproduces the compositional dependence of the Young's modulus of amorphous Cu–Zr alloys at room temperature.[29] In the present study, however, we focused on one particular composition: $Cu_{64.5}Zr_{35.5}$. To begin with, atomic volume and bulk modulus were determined as a function of temperature. For this purpose, we took the model of amorphous $Cu_{64.5}Zr_{35.5}$ alloy from Ref. 29. In the following, this model will be referred to as model 1. The model consists of 25 000 atoms with periodic boundary conditions in all directions. After being equilibrated at $T=300$ K, model 1 was heated in steps of 100 K; at each temperature step the model was equilibrated during 20 000 MD steps (~40.7 ps), followed by averaging the pressure over the next 20 000 MD steps. For each temperature step hydrostatic dilation was applied to increase the model volume by 1%, after which the structure was again equilibrated during 20 000 MD steps. Subsequently, the pressure was averaged over the next 20 000 MD steps. Lastly, another 1% hydrostatic dilatation was applied to obtain the pressure at a third density. This approach yielded pressure as a function of volume for each given temperature, from which the equilibrium atomic volume was determined. The equilibrium model was created at this volume and equilibrated during 20 000 MD steps; subsequently, the properties of model 1 (to be discussed later) were averaged over the next 20 000 MD steps. The above procedure was repeated at temperature increments of 100 K up to $T=1500$ K.

While uniaxial mechanical loading tests are typically used to experimentally examine the deformation behavior of

metallic glasses, it is not reasonable to exactly reproduce this loading configuration in atomistic simulations because the effect of the exposed edges will be much more pronounced due to the relatively small number of atoms. In particular, if free surfaces were employed in the direction normal to the loading axis, as would be the case for simulated uniaxial compression, then there could be significant surface effects due to the limited number of atoms in the simulation (25 000); the sample thickness will only be ~40 Å. Therefore, to help mitigate unnecessary complications (e.g., bending in compression), we utilized a biaxial deformation arrangement. This model, which we refer to as model 2, also consisted of 25 000 atoms and had periodic boundary conditions in the *x*- and *y*-directions and free surfaces in the *z*-direction. Initially, the cross section was 43.4×43.4 Å^2 in the *x*- and *y*-directions, while the length was ~217 Å in the *z*-direction. A compressive strain using a constant strain rate at 700 K was applied in the *x*- and *y*-directions to biaxially deform the model until $\varepsilon_{xx}=\varepsilon_{yy}=-0.1$. In order to examine atomic structure after deformation, the model was unloaded by applying a biaxial tensile strain at the same strain rate until the sum $|\sigma_{xx}+\sigma_{yy}|$ dropped to zero.

Lastly, in order to study the diffusion as a function of atomic density in the amorphous $Cu_{64.5}Zr_{35.5}$ alloy, we created model 3. In this case, the simulation cell consisted of only 5000 atoms, but the model was created in the same manner as discussed previously for model 1, except that due to the relatively small number of atoms in model 3 we were able to anneal it for a much longer time period, 2 000 000 MD steps (4.07 ns), at each temperature.

B. Dynamic mechanical analyzer measurements

In order to experimentally measure the Young's modulus of the $Cu_{64.5}Zr_{35.5}$ alloy as a function of temperature, melt spun ribbons having a cross section of 13.2×0.072 mm^2, which were synthesized at the Materials Preparation Center at Ames Laboratory[30] by quenching onto a Cu wheel rotating at a linear velocity of 25 m/s, were examined using a Netzsch 242C dynamic mechanical analyzer (DMA) in tension mode. The ribbons were heated at 3 K/min from 278 to 823 K, while the tensile load was sinusoidally varied between ~3.5 and 7.0 N at a frequency of 1 Hz. The typical outputs of a DMA experiment are the storage modulus (E') and the loss modulus (E''), where the former relates to the recoverable strain and the latter corresponds to internal energy dissipation. Because metallic glasses typically have such a high elastic strain limit at temperatures below and approaching their glass transition, the E'' contribution during these DMA tests was approximately six orders of magnitude less than the E' signal. In such a situation, the E' data from a DMA measurement are extremely close to the static Young's modulus (E) of the material.

C. High-temperature plastic deformation measurements

In order to prepare suitable "bulk" samples for uniaxial compression testing, a $Cu_{64.5}Zr_{35.5}$ ingot was first prepared by arc melting high-purity Cu and Zr together in an argon environment. Subsequently the ingot was induction melted in a fused silica tube and injection cast into a water-cooled copper mold to form a rod 1 mm in diameter and approximately 25 mm in length. The amorphous nature of the as-cast rods was confirmed using high-energy x-ray scattering (not shown) at the MU-CAT beamline at the Advanced Photon Source (APS). Samples with a length/diameter ratio of 2:1 were cut from the as-cast rod for plastic deformation experiments. Prior to loading, the samples were annealed at 698 K, which is nominally 60 K below the glass transition temperature, for 270 min to allow for structural relaxation. Uniaxial compression tests were performed at a constant strain rate of 10^{-4} s^{-1} at 698 K in a Zwick Z050 load frame. The strain in the sample was measured by a linear inductive differential transducer with an accuracy of ±15 nm.

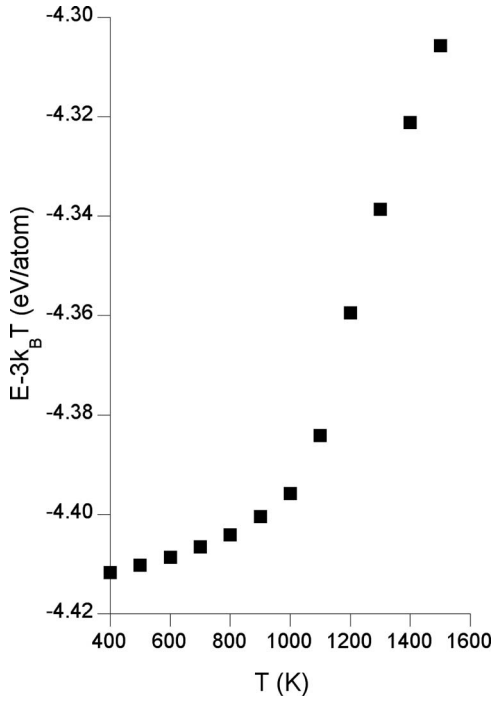

FIG. 1. Energy as a function of temperature.

III. RESULTS AND DISCUSSION

A. Temperature dependence of elastic properties

In this section, we present the data obtained using model 1. The total (i.e., potential+kinetic) energy of the system as a function of temperature for the glass model is shown in Fig. 1. The curve exhibits two distinct regimes at lower and higher temperatures, which correspond, respectively, to the amorphous solid and the supercooled liquid. The glass transition temperature (T_g) can be estimated as ~1000 K based on these data, while the T_g determined experimentally by constant-rate (40 K/min) differential scanning calorimetry (DSC) is ~760 K. It should be noted that the interatomic potential development procedure did not incorporate fitting to the thermal data; therefore, the difference in T_g is not fully unexpected. It should be also noted that given the several orders-of-magnitude difference in the heating rates between the DSC experiments and the MD simulations, the T_g corre-

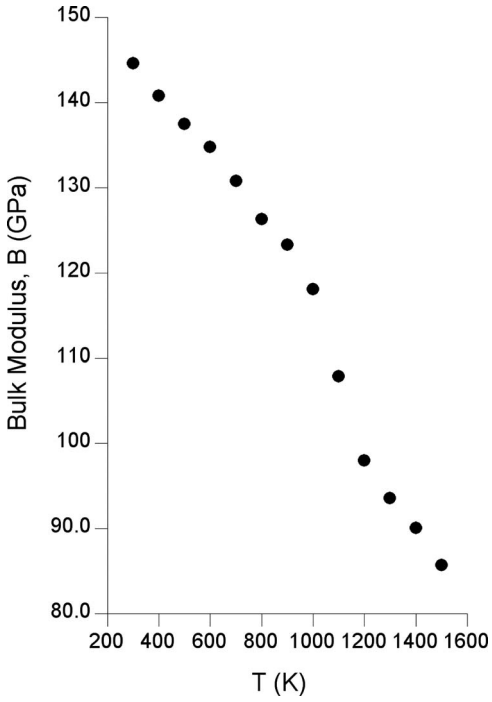

FIG. 2. Bulk modulus as a function of temperature.

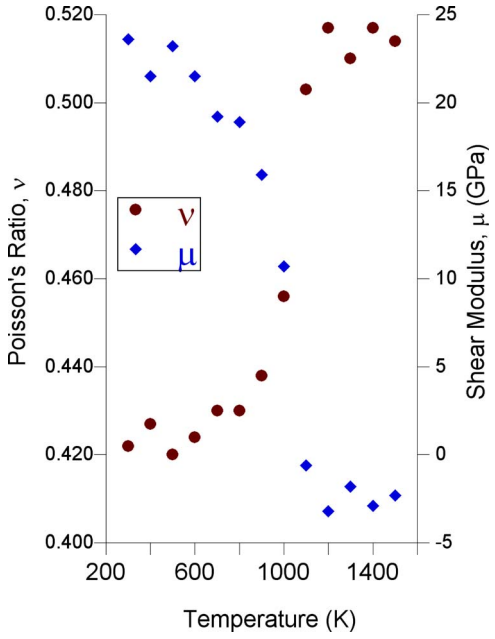

FIG. 3. (Color online) Poisson's ratio and shear modulus as a function of temperature.

sponding to the experimental heating rate should be lower than that obtained in MD simulation (e.g., see Ref. 31 for further discussion). While the potential from Ref. 26 predicts a higher T_g than experimentally measured, it does indeed predict an amorphous solid at $T=700$ K, making it suitable for the purposes of the present study.

The elastic properties of the amorphous solid and the supercooled liquid as a function of temperature were examined for model 1. The bulk modulus (Fig. 2) decreases almost linearly with increasing temperature for the amorphous solid and exhibits a marked change in slope around 1000 K, which corresponds to T_g. Above this temperature, the bulk modulus of the supercooled liquid decreases almost linearly with increasing temperature. The technique for calculating Poisson's ratio and shear modulus from our MD simulations is described in detail in an earlier report.[29] In this method, a uniaxial strain in one (z) direction is applied while the model size in x- and y-directions is kept fixed, and the resulting stress (σ_{zz}) is determined during MD simulation. Using this approach, we find that the temperature dependences of the Poisson's ratio and shear modulus (Fig. 3) clearly display a transition between the amorphous solid to the supercooled liquid at $T\sim1000$ K. Note that Duan *et al.*[24] performed MD simulations on a metallic glass richer in Zr, $Zr_{54}Cu_{46}$ and found comparable decreases in bulk and shear moduli with increasing temperatures below T_g. Between 300 and 500 K, the values of these two elastic constants are considerably higher in the $Cu_{64.5}Zr_{35.5}$ alloy examined in our study. This is not surprising because we have previously shown that the elastic constants of Cu–Zr glasses are strongly dependent on alloy composition.[29]Also, the quench rate in Ref. 24 was approximately ten times higher than in our work, which could also have an effect due to configurational relaxation differences. It is interesting to note that for our $Cu_{64.5}Zr_{35.5}$ metallic glass, the calculated Poisson's ratio for the supercooled liquid is a little higher than 0.5 and the shear modulus is slightly negative. Obviously, the results above $T=1000$ K are not physically reasonable but rather indicate the magnitude of the error associated with the uncertainty in determining of σ_{zz}. Three possible factors contributing to this uncertainty are the following: (1) there is uncertainty associated with the final model size and fluctuation of σ_{zz} during the MD simulation; (2) we applied the strain of 0.5% and it is possible that there are deviations from linear elasticity at such strain; and (3) it is possible that the time during which model 1 was allowed to relax was insufficient to achieve equilibrium. Regardless of the uncertainty associated with the method, the Poisson's ratio and shear modulus exhibit distinct changes at $T\sim1000$ K, which are much larger than the magnitude of the error values; therefore, we conclude that this temperature does indeed correspond to T_g for our model. The glass transition phenomenon may be further seen in the plot of the atomic volume of model 1 as a function of temperature (Fig. 4), which, similar to the elastic constants, shows a distinct change in slope at ~1000 K, corresponding to the T_g of our simulated glass model.

To determine the validity of the predicted glass properties for model 1, we compared the simulation data with the elastic modulus of the $Cu_{64.5}Zr_{35.5}$ melt spun ribbons measured using DMA tests (see Sec. II B). Figure 5 displays the Young's modulus as a function of temperature determined by MD simulations and DMA tests. The upper-right inset illustrates that the temperature dependence of the elastic modulus determined by the MD simulations is in good agreement with the experimental measurements, which is especially encouraging since as explained earlier no information about elastic properties was used while developing the interatomic potential described in Ref. 27.

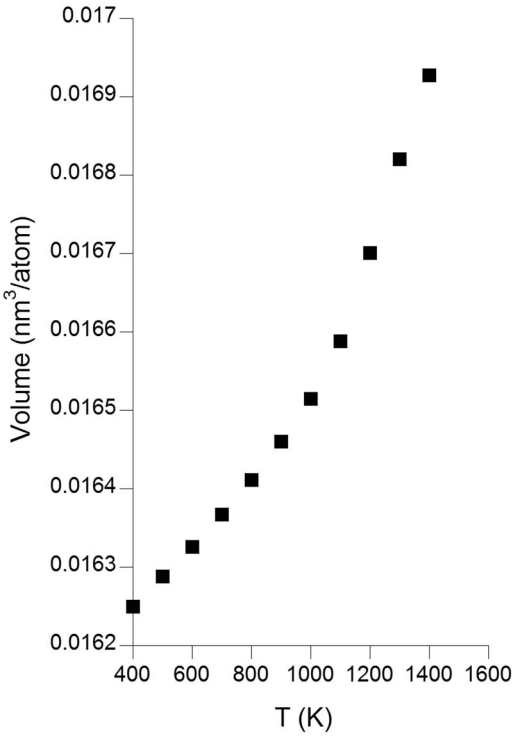

FIG. 4. Atomic volume as a function of temperature.

B. High-temperature deformation behavior of amorphous $Cu_{64.5}Zr_{35.5}$

The close agreement between the experimentally measured Young's modulus at $T=700$ K and that predicted for the simulated glass, model 1, suggests that the interatomic potentials accurately capture the high-temperature elastic deformation behavior of the $Cu_{64.5}Zr_{35.5}$ alloy. To examine the high-temperature ($T=700$ K) plastic deformation behavior of this alloy, model 2 (periodic boundary conditions in x- and y-directions only) was deformed in biaxial compression. As discussed previously, the biaxial loading geometry was utilized to minimize edge effects. In this loading scheme, the stress component along the z-direction, σ_{zz}, should be zero, while σ_{xx} and σ_{yy} should be the same. In reality, because of the small model size, the σ_{xx} and σ_{yy} stress components are not exactly the same; therefore, we used their average value

$$\bar{\sigma} = (\sigma_{xx} + \sigma_{yy})/2. \tag{1}$$

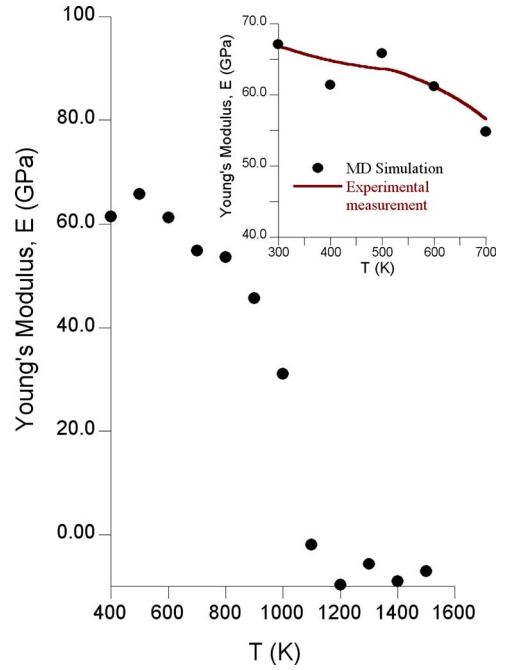

FIG. 5. (Color online) Young's modulus obtained from MD simulation as a function of temperature. The inset shows the comparison with experimental data.

Figure 6(a) shows the stress-strain curves obtained from the MD simulations at two different strain rates. For applied strains less than ~0.02, the stress increases linearly with increasing applied strain, corresponding to elastic deformation. For comparison to theoretical Hookean behavior, refer to the black line in Fig. 6(a), which was derived using the Young's modulus and Poisson's ratio obtained using model 1. Within the linear region (i.e., $\varepsilon < \sim 0.018$) the stress-strain curve for the biaxial compression of model 2 is in good agreement with the predicted response calculated from elastic constants using model 1. For higher applied strains the deformation becomes nonlinear, which corresponds to the onset of plastic flow. The stress reaches a maximum, followed by a decrease with increasing applied strain until approaching a steady-state value. The stress-strain curves obtained at the two strain rates illustrate that the flow stress of the simulated metallic glass increases with increasing strain rate. The transition between the elastic and plastic deformation regimes is further seen in the inset of Fig. 6(a), which shows the measured inelastic (anelastic+plastic) strain as a function of the applied strain. To measure the inelastic strain we took several snapshots of the model during compression at a strain rate of 4.9×10^6 s^{-1}. Immediately following each incremental compressive loading step, this model was unloaded by applying a tensile strain at the same strain rate until the sum $|\sigma_{xx}+\sigma_{yy}|$ dropped to zero for each snapshot, thus removing the elastic component from the total strain. The remaining inelastic strain component is then defined as $\varepsilon_{\text{inelastic}}=|L_{x,y}-L^0_{x,y}|/L^0_{x,y}$, where $L^0_{x,y}$ is the dimension of the simulation cell before deformation and $L_{x,y}$ is the size of the simulation cell after the loading-unloading cycle (note that in the preceding the subscripts x and y correspond, respectively, to the cell length of model 2 in the x- and y-directions). As can be seen from Fig. 6(a), the inelastic strain is almost zero when applied strain is less than 1.5%.

It should be noted that quantitative agreement between the MD simulations and the experimental plastic deformation tests is not expected due to the dramatic difference in the strain rates. Furthermore, there are also differences related to the fact that the employed potential does not accurately predict the liquid-glass transition temperature and that the glass models created in MD simulation at best correspond to as-cast glass samples rather than the structurally relaxed samples utilized in the t experiments. Additionally, the loading conditions in MD simulation and experiment are different (uniaxial versus biaxial). However, if MD simulation

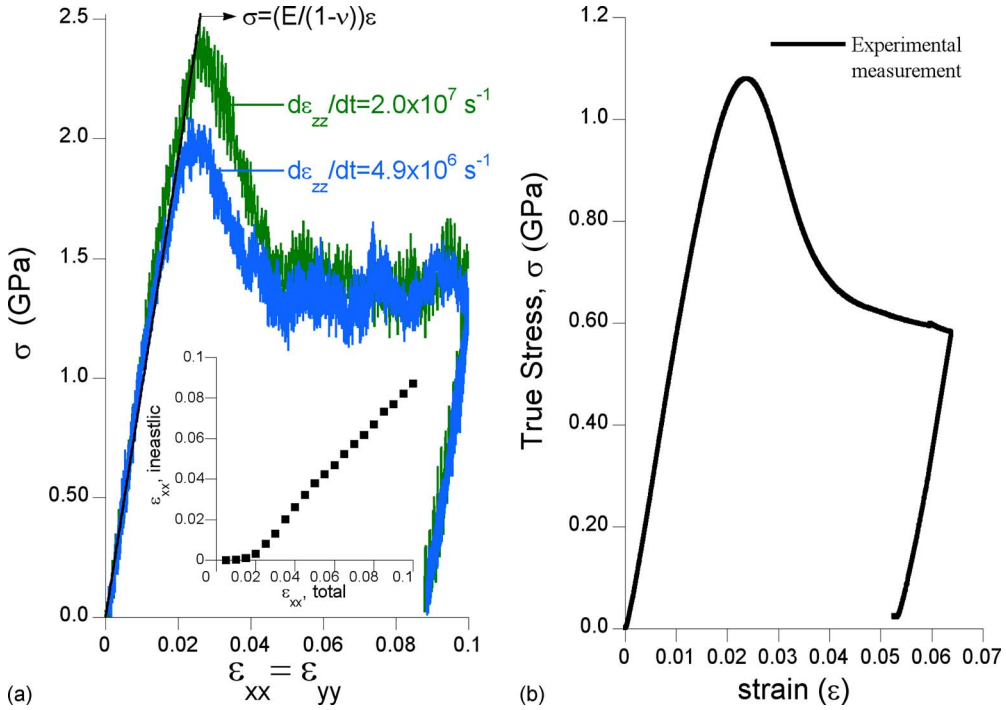

FIG. 6. (Color online) (a) $|\bar{\sigma}|=(\sigma_{xx}+\sigma_{yy})/2$ as a function of applied strain obtained from MD simulations of biaxial compression at 700 K using two different strain rates; black straight line shows Hookean behavior using the Young's modulus and Poisson's ratio determined from model 1. The lower inset shows inelastic strain variation as a function of total strain along the *x*-direction and (b) true stress-strain data from deformation experiment at 698 K using a strain rate of 10^{-4} s^{-1}.

captures the most important qualitative features of plastic deformation, it can be used to explore the atomic mechanisms associated with plastic flow.

For comparison with the stress-strain curves determined from the MD simulations, an experimental deformation test was performed using 1 mm rods of $Cu_{64.5}Zr_{35.5}$ metallic glass, which were deformed in uniaxial compression at a constant strain rate of 1×10^{-4} s^{-1} at 698 K (see Sec. II C). Since the strain rate utilized in the MD simulations is several orders of magnitude larger than the experimental strain rate, the predicted flow stress for the simulated metallic glass is higher than that measured experimentally [Fig. 6(b)]. Despite the large differences in strain rates, the elasto-plastic responses of the simulated glass and the 1 mm rods both exhibit a maximum stress, followed by flow softening with increasing strain and steady-state plastic flow at higher strains. Flow softening following yielding of homogeneously deformed metallic glasses within the non-Newtonian regime has been attributed to an increase in the free volume, which decreases the viscosity.[32,33] This increase in free volume associated with plastic deformation has been confirmed through both density[34] and heat capacity measurements.[12,35] Following the flow softening seen in both the MD simulations and the experimental compression tests, the stresses approach plateau values with increasing strain. This steady-state flow regime corresponds to a dynamic equilibrium between the creation and annihilation of free volume.[33,36] The good qualitative agreement between the plastic deformation behavior predicted by the MD simulations and that measured experimentally suggests that in spite of the dramatic difference in the strain rate, the simulation appears to properly capture the atomic dynamics during deformation.

To further examine the mechanisms of deformation, we calculated the atomic volume as a function of applied strain for the simulated glass deformed at two different strain rates. Recall that the simulation cell for model 2 had free surfaces in the *z*-direction, which precluded accurately defining the cell length in the *z*-direction. As a consequence, we could not define the atomic volume simply as the ratio of the simulation cell volume to the number of atoms. To account for this, we ignored the 200 atoms that were closest to the two free surfaces and determined the cell length in the *z*-direction L_z' as the distance between minimal and maximal *z*-coordinates of the remaining 24 800 atoms. With this approach, atomic volume was defined as $V_a=L_xL_yL_z'/24\,800$. As seen in Fig. 7, at applied strains below the respective yield points, the atomic volumes decrease with increasing strain, consistent with compressive elastic deformation. Following the onset of plastic flow, however, the atomic volumes reach minimum values corresponding to the maximum stress on the corresponding stress-strain curves shown in Fig. 6(a). Interestingly, for both strain rates the atomic volume increases within the flow-softening regime of the stress-strain curves, suggesting perhaps that the stress drop is associated with an increase in free volume throughout the atomic structure.[13] Furthermore, the magnitude of the increase in atomic volume following yielding increases with increasing strain rate, which is consistent with experimental observations for homogeneously deformed multicomponent glasses.[13,33] For the two different strain rates, both the atomic volume and the stress approach plateau values for applied strains above ~0.06. As discussed before, this plateau regime has been attributed to a dynamic equilibrium between the creation and annihilation of free volume. For the glass model deformed at

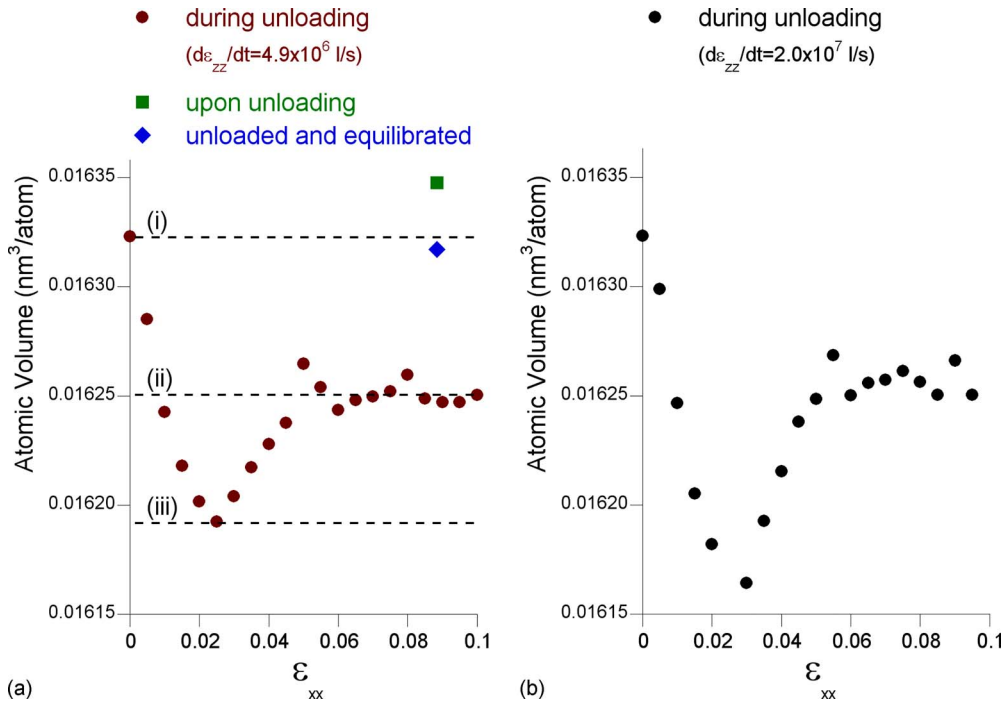

FIG. 7. (Color online) Atomic volume vs applied strain at an applied strain rate of (a) 4.9×10^{6} 1/s and (b) 2.0×10^{7} 1/s. See text for explanation of square and diamond symbols in (a).The dashed horizontal lines in (a) correspond to volume of model 2 as follows: (i) prior to loading, (ii) during "steady-state" plastic deformation, and (iii) at the point of minimum volume (i.e., maximum density). The regimes defined by lines [(i)–(iii)] in (a) are indicated later in Fig. 10.

a strain rate of 4.9×10^{6} s^{-1}, we find that after removal of the elastic strain, the atomic volume returns to a slightly higher value (square symbol at ~0.016 34 nm^3/atom) than the initial atomic volume of the undeformed glass, which is indicated by the dashed horizontal line labeled (i) in Fig. 7(a). After the unloaded structure is allowed to equilibrate at 700 K during 6.1 ns, the atomic volume returns to approximately the same level as before deformation (diamond symbol at ~0.016 318 nm^3/atom), indicating that some structural relaxation has occurred and, as a consequence, a significant portion of the free volume that was created during plastic flow has been annihilated.

To explore the nature of the free volume creation during plastic deformation, we calculated the size distribution of spherical open volume regions (cavities) in the simulated glass, model 2. To determine the size of these cavities, we assumed that all Cu and Zr atoms are hard spheres with respective radii of 1.25 and 1.60 Å; note that these radii were determined from the positions of the first peaks in the corresponding partial pair correlation functions, which are not shown here. The radius of a cavity is defined as the maximum radius of a sphere that can be inserted into the model without intersecting any Cu or Zr atoms. The distributions of the cavity radii at different applied strains for the simulated glass deformed at a strain rate of 4.9×10^{6} s^{-1} are displayed in Fig. 8. The results reveal that very few spherical cavities having radii greater than 0.6 Å are present in the atomic structure. Sietsma and Thijsse[36] examined the distribution of open volume regions in a simulated Pd–Ni–P structure obtained from reverse Monte Carlo simulations of experimental radial distribution functions. From their analysis, they determined that the cavities could be divided into two types: intrinsic voids, which were similar to Bernal holes, and larger holes that could be removed with annealing. Furthermore, they found that the larger holes were largely nonspherical (i.e., dissimilar to crystalline vacancies). Similarly, using positron annihilation spectroscopy, Flores *et al.*[37] also found that large, open-volume regions with sizes similar to vacancies were present in inhomogeneously deformed Zr–

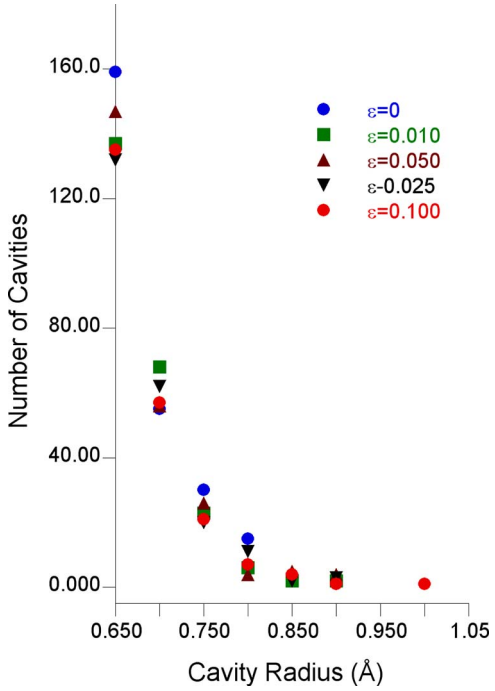

FIG. 8. (Color online) Cavity distribution for different strains at the strain rate of 4.9×10^{6} 1/s.

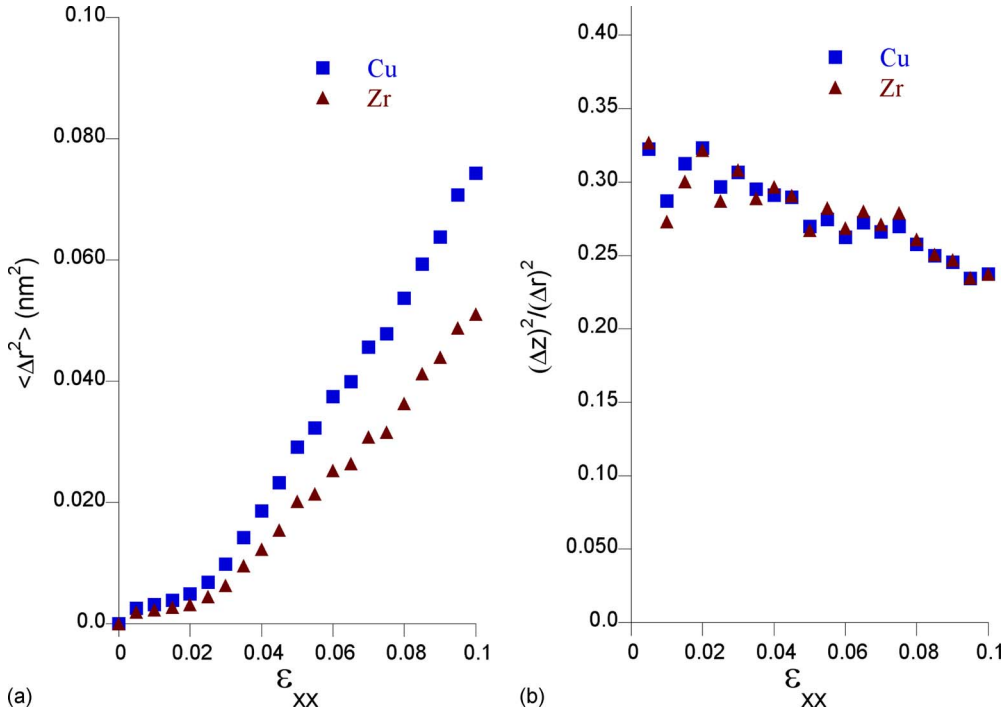

FIG. 9. (Color online) (a) MSD of atoms during deformation and (b) the ratio of the MSD in the z-direction to the MSD in all directions.

Cu–Ni–Al–Nb metallic glass. Since such a high concentration of discrete vacancies is unlikely in the glass structure, they concluded that the open volume must be distributed more diffusely among small collections of atoms, which argon referred to as shear transformation zones.[6] The cavity size distributions shown in Fig. 8. also suggest that the free volume associated with plastic deformation does not create large spherical holes. Moreover, the plot shows that the concentration of the cavities is not dependent on the magnitude of the applied strain, further suggesting that the free volume created during deformation is not in discrete spherical sites such as the case for crystalline vacancies.

In order to analyze the effect of the applied strain on the atomic mobility, we transformed the size of each biaxially deformed model 2 snapshot back to their original size. This approach seeks to separate out the atomic displacements associated specifically with uniform elastic and plastic straining. The atomic displacements were calculated as the difference in the atom position in the initial model and snapshot under consideration. The calculated mean square displacements (MSDs) of all atoms as a function of applied strain are shown in Fig. 9(a), which demonstrates that the MSD of the atoms exhibits a large increase following the onset of plastic flow ($\varepsilon \sim 0.020$), corresponding to a significant acceleration in the atomic mobility. To examine if this large increase in the MSD of the atoms was the result of diffusion directionally biased by the applied strain, we calculated the ratio of the MSD in the z-direction to overall MSD [Fig. 9(b)]. The relative MSD in the z-direction shows little change following the onset of plastic flow; therefore, we conclude that the atomic mobility is not directionally biased.

The large increase in the atomic mobility following plastic flow cannot be explained by the increase in the free volume associated with plastic flow if this additional free volume is homogeneously distributed. Indeed this is illustrated in Fig. 10, which shows the diffusivities of Cu and Zr as a function of the average atomic volume. The data were obtained from model 3, which had periodic boundary conditions in all directions that were each subject to pure dilatation. Although the data are noisy due to the relatively small model size and low temperature of the simulation, it is clear that the change in mobility associated with the change in the

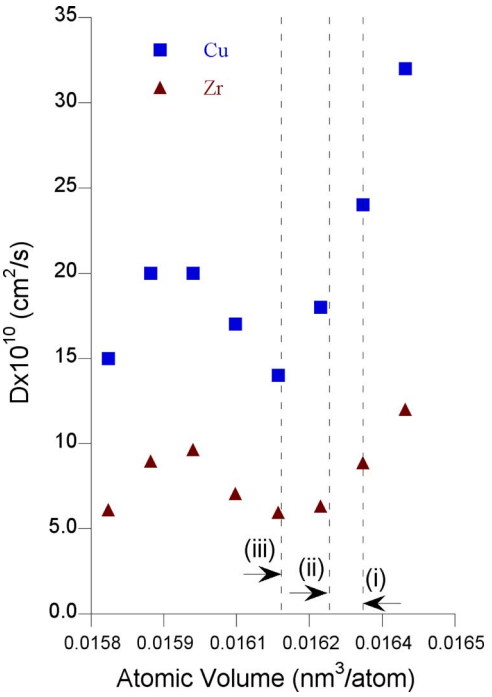

FIG. 10. (Color online) Diffusion as function of atomic volume under applied pure hydrostatic dilatation. The vertical dashed lines correspond to the regimes defined in the caption for Fig. 7(a).

atomic volume shown in Fig. 7 cannot exceed ~50%; the portion of Fig. 10 represented by the volume change during deformation in Fig. 7 is indicated by the vertical lines. In contrast Fig. 9 demonstrates an increase in diffusivity of ~300%. Thus, if the increase in the atomic mobility during plastic flow is associated with the increase in free volume, analysis of Figs. 7 and 10 suggests that the increase in free volume during plastic deformation is not uniformly distributed but instead is more or less localized among clusters of atoms. The nature of the free volume distribution is the subject of continuing simulations.

IV. CONCLUSIONS

Using a new EAM FS interatomic potential for the Cu–Zr alloy system, we performed MD simulations to determine the elastic constants of a $Cu_{64.5}Zr_{35.5}$ amorphous alloy as a function of temperature. From the simulations we find that the elastic constants exhibit an approximately linear temperature dependence for temperatures below 1000 K, which corresponds to the glass-transition temperature of our simulated 25 000-atom model structure. Above T_g, the elastic constants of the supercooled liquid also exhibit almost linear temperature dependence, albeit of different magnitudes than the amorphous solid. Experimental measurements of the Young's modulus as a function of temperature using DMA are in good agreement with the predicted temperature dependence from the MD simulations, supporting the accuracy of the interatomic potentials. Furthermore, the high-temperature plastic deformation behavior determined by the MD simulations compares well with the data from plastic deformation experiments performed on $Cu_{64.5}Zr_{35.5}$ metallic glass rods at 698 K. The MD simulations reveal that the flow softening regime of the stress-strain curve corresponds to an increase in the free volume in the atomic structure. Moreover, analysis of the MSDs of the atoms in the structure shows that the atomic mobility in the alloys significantly increases in the same regime. However, this increase in diffusion cannot be solely attributed to the increase in free volume.

ACKNOWLEDGMENTS

The authors gratefully acknowledge Dr. M. Meyer at Netzsch Instruments, Selb, Germany for performing the DMA studies and Dr. Eun Soo Park, Harvard University, Cambridge, MA for synthesizing the 1 mm diameter $Cu_{64.5}Zr_{35.5}$ amorphous samples used in the homogeneous deformation experiments. Work at the Ames Laboratory was supported by the Department of Energy, Office of Basic Energy Sciences under Contract No. DE-AC02-07CH11358. The high-energy x-ray work at the MUCAT sector of the APS was supported by the U.S. Department of Energy, Office of Science, Basic Energy Sciences under Contract No. DE-AC02-06CH11357.

[1] O. P. Bobrov, K. Csach, S. V. Khonik, K. Kitagawa, S. A. Lyakhov, M. Y. Yazvitsky, and V. A. Khonik, Scr. Mater. **56**, 29 (2007).
[2] H. Kato, Y. Kawamura, A. Inoue, and H. S. Chen, Mater. Trans., JIM **41**, 1202 (2000).
[3] H. Kato, Y. Kawamura, A. Inoue, and H. S. Chen, Appl. Phys. Lett. **73**, 3665 (1998).
[4] A. I. Taub, Acta Metall. **28**, 633 (1980).
[5] A. I. Taub and F. Spaepen, Scr. Metall. **14**, 1197 (1980).
[6] A. S. Argon, Acta Metall. **27**, 47 (1979).
[7] H. S. Chen, Scr. Metall. **7**, 931 (1973).
[8] F. Spaepen, Scr. Mater. **54**, 363 (2006).
[9] F. Spaepen, Acta Metall. **25**, 407 (1977).
[10] M. H. Cohen and D. Turnbull, J. Chem. Phys. **31**, 1164 (1959).
[11] A. van den Beukel, S. Vanderzwaag, and A. L. Mulder, Acta Metall. **32**, 1895 (1984).
[12] P. de Hey, J. Sietsma, and A. van den Beukel, Mater. Sci. Eng., A **226-228**, 336 (1997).
[13] P. de Hey, J. Sietsma, and A. van den Beukel, Acta Mater. **46**, 5873 (1998).
[14] M. L. Falk and J. S. Langer, Phys. Rev. E **57**, 7192 (1998).
[15] Y. F. Shi, M. B. Katz, H. Li, and M. L. Falk, Phys. Rev. Lett. **98**, 185505 (2007).
[16] Y. F. Shi and M. L. Falk, Phys. Rev. Lett. **95**, 095502 (2005).
[17] M. S. Daw and M. I. Baskes, Phys. Rev. B **29**, 6443 (1984).
[18] M. W. Finnis and J. E. Sinclair, Philos. Mag. A **50**, 45 (1984).
[19] K. W. Jacobsen, J. K. Norskov, and M. J. Puska, Phys. Rev. B **35**, 7423 (1987).
[20] Y. Li, JOM **57**, 60 (2005).
[21] D. Wang, Y. Li, B. B. Sun, M. L. Sui, K. Lu, and E. Ma, Appl. Phys. Lett. **84**, 4029 (2004).
[22] G. Duan, D. H. Xu, Q. Zhang, G. Y. Zhang, T. Cagin, W. L. Johnson, and W. A. Goddard, Phys. Rev. B **71**, 224208 (2005).
[23] A. Paduraru, A. Kenoufi, N. P. Bailey, and J. Schiotz, Adv. Eng. Mater. **9**, 505 (2007).
[24] G. Duan, M. L. Lind, M. D. Demetriou, W. L. Johnson, W. A. Goddard, T. Cagin, and K. Samwer, Appl. Phys. Lett. **89**, 151901 (2006).
[25] M. Wakeda, Y. Shibutani, S. Ogata, and J. Park, Intermetallics **15**, 139 (2007).
[26] M. I. Mendelev, D. J. Sordelet, and M. J. Kramer, J. Appl. Phys. **102**, 043501 (2007).
[27] M. I. Mendelev, M. J. Kramer, C. A. Becker, and M. Asta, Philos. Mag. **88**, 1723 (2008).
[28] M. I. Mendelev and G. J. Ackland, Philos. Mag. Lett. **87**, 349 (2007).
[29] M. I. Mendelev, D. K. Rehbein, R. T. Ott, M. J. Kramer, and D. J. Sordelet, J. Appl. Phys. **102**, 093518 (2007).
[30] Materials Preparation Center, Ames Laboratory, US DOE Basic Energy Sciences, Ames, IA, USA, available from www.mpc.ameslab.gov.
[31] M. Kluge and H. R. Schober, Phys. Rev. B **70**, 224209 (2004).
[32] U. Harms, O. Jin, and R. B. Schwarz, J. Non-Cryst. Solids **317**, 200 (2003).
[33] M. Heggen, F. Spaepen, and M. Feuerbacher, J. Appl. Phys. **97**, 033506 (2005).
[34] A. van den Beukel and J. Sietsma, Acta Metall. Mater. **38**, 383 (1990).
[35] S. S. Tsao and F. Spaepen, Acta Metall. **33**, 881 (1985).
[36] J. Sietsma and B. J. Thijsse, Phys. Rev. B **52**, 3248 (1995).
[37] K. M. Flores, B. P. Kanungo, S. C. Glade, and P. Asoka-Kumar, J. Non-Cryst. Solids **353**, 1201 (2007).